



Sources and accumulation of plutonium in a large Western Pacific marginal sea: The South China Sea



Junwen Wu^a, Minhan Dai^{a,*}, Yi Xu^a, Jian Zheng^b

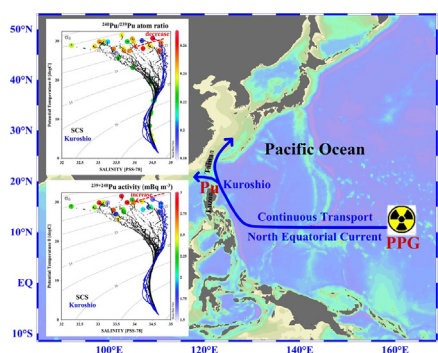
^a State Key Laboratory of Marine Environmental Science, Xiamen University, Xiang'an District, Xiamen 361102, China

^b Fukushima Project Headquarters, National Institute of Radiological Sciences, National Institutes for Quantum and Radiological Science and Technology, 491 Anagawa, Inage, Chiba 263-8555, Japan

HIGHLIGHTS

- ~41% of Pu in the SCS is sourced from the PPG via the NEC and Kuroshio Current.
- There occurred enhanced scavenging of Pu sourced from the PPG.
- There occurred significant accumulation of Pu in the SCS.

GRAPHIC ABSTRACT



ARTICLE INFO

Article history:

Received 26 May 2017

Received in revised form 25 July 2017

Accepted 25 July 2017

Available online xxx

Editor: Jay Gan

Keywords:

Plutonium

South China Sea

Pacific Proving Grounds

$^{240}\text{Pu}/^{239}\text{Pu}$ atom ratio

Scavenging

Accumulation

ABSTRACT

In order to examine the sources of plutonium (Pu) and elaborate its scavenging and accumulation processes, $^{240}\text{Pu}/^{239}\text{Pu}$ atom ratios and $^{239} + ^{240}\text{Pu}$ activities in the water column of the South China Sea (SCS) were determined and compared with our previously reported data for the sediments. Consistently high $^{240}\text{Pu}/^{239}\text{Pu}$ atom ratios that ranged from 0.184–0.250 (average = 0.228 ± 0.015), indicative of non-global fallout Pu sources were observed both in the surface water and at depth during 2012–2014. The spatial distribution of the $^{240}\text{Pu}/^{239}\text{Pu}$ atom ratio in the SCS showed a decreasing trend away from the Luzon Strait, which was very consistent with the introduction pathway of the Kuroshio Current. The Kuroshio had an even heavier Pu isotopic ratio ranging from 0.250–0.263 (average = 0.255 ± 0.006), traceable to the non-global fallout Pu signature from the Pacific Proving Grounds (PPG). Using a simple two end-member mixing model, we further revealed that this PPG source contributed $41 \pm 17\%$ of the Pu in the SCS water column. The $^{239} + ^{240}\text{Pu}$ activities in the SCS surface seawater varied from 1.59 to 2.94 mBq m^{-3} , with an average of $2.34 \pm 0.38 \text{ mBq m}^{-3}$. Such an activity level was ~40% higher than that in the Kuroshio. The distribution of $^{239} + ^{240}\text{Pu}$ in the surface seawater further showed a general trend of increase from the Kuroshio to the SCS basin, suggesting significant accumulation of Pu within the SCS. The $^{239} + ^{240}\text{Pu}$ inventory of the water column in the SCS basin at the SEATS station with a total depth of ~3840 m was estimated to be ~29 Bq m^{-2} , which was substantially higher than the sediment core estimates made for the SCS basin (3.75 Bq m^{-2}) but much lower than the sediment core estimates made for the shelf of the northern SCS (365.6 Bq m^{-2}). Such differences were determined by the lower scavenging efficiency of Pu in the SCS basin compared to the northern SCS shelf.

© 2017 Elsevier B.V. All rights reserved.

* Corresponding author.

E-mail address: mdai@xmu.edu.cn (M. Dai).

1. Introduction

The input of plutonium (Pu), a man-made element, into the oceanic environment is mainly through above ground nuclear weapons testing (Sholkovitz, 1983), accidental releases (Zheng et al., 2012) and discharges from reprocessing plants (Kershaw et al., 1995; Dai et al., 2005). Because of their high toxicity, long half-lives and a large risk for internal radiation exposure, the fate of Pu isotopes in the ocean is thus of great environmental concern. Note that, when deposited in the ocean, Pu takes part in a series of oceanic processes and can be transported quite far from the source point. Such environmental impact can be beyond a regional scale because of this transport (Buesseler et al., 2017).

The relative abundances of Pu isotopes, typically ^{239}Pu and ^{240}Pu , can be commendably used to trace the special sources of Pu because $^{240}\text{Pu}/^{239}\text{Pu}$ atom ratios vary with reactor types, neutron flux and energy, nuclear fuel burn-up time, and for fallout from nuclear detonations, weapon types and yield (Wu et al., 2014 and references therein). Our previous study concerning the $^{239} + ^{240}\text{Pu}$ activities and $^{240}\text{Pu}/^{239}\text{Pu}$ atom ratios in sediments of the Northern South China Sea (NSCS) and its adjacent Pearl River Estuary (PRE) infers that Pu in the NSCS is sourced from a combination of global fallout with a characteristic $^{240}\text{Pu}/^{239}\text{Pu}$ atom ratio of 0.180 ± 0.014 (Kelley et al., 1999) and close-in fallout traceable to the Pacific Proving Grounds (PPG) in the Marshall Islands that has a very high $^{240}\text{Pu}/^{239}\text{Pu}$ atom ratio of 0.30–0.36 (Buesseler, 1997; Muramatsu et al., 2001) derived from the above-ground nuclear weapons testing carried out during the period 1952–1958 (Wu et al., 2014 and references therein). The present study aimed to further examine if there is a continuously supplying Pu source from the PPG transported via the North Equatorial Current (NEC) and the Kuroshio Current into the SCS through determination of the Pu activity and its isotopic ratio in the water column of the SCS, and to elaborate the scavenging and accumulation of Pu, which is of great importance to understanding the fate of this artificial radionuclide of environmental concerns. We point out that information on Pu activity levels and isotopic ratios would also help in establishing a baseline for future environmental risk assessment related to nuclear power plant operations that see a dramatically increasing rate along the coast of the region (Zeng et al., 2016).

2. Materials and methods

2.1. Study area

The SCS, with a total surface area of $3.5 \times 10^6 \text{ km}^2$, is the largest marginal sea of the North Pacific Ocean. The East Asian monsoon prevails in the SCS leading to a seasonal alternation of surface circulation with a cyclonic gyre in winter (November to March) and an anti-cyclonic gyre in summer (June to September) (Shaw and Chao, 1994). The basin-wide surface circulation gyres effectively reduce the influence of terrestrial inputs on the SCS proper. As a result, the SCS basin has oligotrophic characteristics similar to those of major ocean basins, with low surface chlorophyll-a levels and low primary production rates (Liu et al., 2002; Dai et al., 2013). In contrast, the nearshore area and the continental shelf are more productive (Han et al., 2012; Dai et al., 2014). In addition, the SCS has a unique circulation pattern with dynamic exchanges with the western North Pacific Ocean (WNPO) via the Luzon Strait with a sill depth of ~2000 m. A branch of the Kuroshio Current intrudes from the WNPO into the SCS in the upper layer (~400 m) and transports westward along the northern continental slope of the SCS, the SCS water outflows into the WNPO in the intermediate layer (~500–1500 m) and the WNPO deep water flows again into the SCS in the deeper layer (~1500 m) (Tian et al., 2006; Liu et al., 2014; Wu et al., 2015).

The Kuroshio is the important western ocean boundary current. It originates from the northward bifurcation of the NEC which flows westward to the Philippine Sea (Wang et al., 2011; Centurioni et al., 2004).

The Kuroshio intrusion to the SCS through the Luzon Strait presents a seasonal pattern with the intrusion being stronger in winter than in summer (Shaw, 1991), and significantly modulates the surface seawater chemistry of the NSCS (Du et al., 2013; Wu et al., 2015).

2.2. Sample collection

Sampling was conducted onboard the R/V *Dongfanghong II* in spring and summer 2012, and in spring 2014. The sampling locations are shown in Fig. 1 and in Table 1. Depth profile samples were collected at the South-East Asian Time Series Stations (SEATS) located in the northern basin of the SCS in April (0–300 m, SEATS I) and in August 2012 (0–1000 m, SEATS II). The remaining samples were all collected from the surface. The surface samples were collected in clean plastic buckets using a built-in pumping system, and subsurface samples were collected in Niskin bottles on a CTD rosette system. Upon collection, about 100 L unfiltered seawater samples were acidified with concentrated HNO_3 to a pH of about 1.6 for the subsequent sample processing and Pu measurements. Adding concentrated HNO_3 to a pH of about 1.6 can destroy any hydrolysis products or complexes of Pu and favors the formation of oxidized Pu (V–VI) in the seawater (Choppin, 2006, 2007).

2.3. Sample processing and Pu isotope analysis

The analytical procedure used for $^{239} + ^{240}\text{Pu}$ in seawater was in accordance with Bu et al. (2014a). Briefly, a known amount of ^{242}Pu (IRMM-085, European Commission Joint Research Centre, Belgium) was added to the seawater samples as a yield monitor. The Pu in the spiked sample was co-precipitated with ferric hydroxide ($\text{Fe}(\text{OH})_3$) by adding ~10 mL Fe^{3+} solution (15.5 mg mL^{-1}) and adjusting to pH ~9 with the addition of concentrated NH_4OH . The precipitate was dissolved in 20 mL 8 M HNO_3 and Pu was adjusted to Pu^{4+} through adding NaNO_2 . The Pu in the sample solution was subsequently purified with two-stage anion-exchange columns using AG 1-X8 and AG MP-1 M (Bio-Rad) (Bu et al., 2014b). The final sample solution, evaporated to near dryness was dissolved in 4% ultrapure HNO_3 (1.0 mL) and filtered for MC-ICP-MS analysis. The determination of Pu isotopes was conducted, using MC-ICP-MS (Nu plasma HR, Nu Instruments Ltd., England) in a low resolution mode in order to obtain the maximal sensitivity, in the State Key Laboratory of Marine Environmental Science, Xiamen University. The DSN-100 high efficiency sample introduction system with a membrane de-solvation unit and a conical concentric nebulizer was used. The chemical yield for Pu was $62.1 \pm 10.7\%$. We obtained high precisions of $^{239} + ^{240}\text{Pu}$ activity and $^{240}\text{Pu}/^{239}\text{Pu}$ atom ratio in seawater, i.e., their relative standard deviations of the uncertainties were $1.6 \pm 1.0\%$ and $2.4 \pm 1.8\%$. This was significantly superior to the values measured using SF-ICP-MS (corresponding to $11.9 \pm 5.6\%$ and $13.0 \pm 4.3\%$) (Bu et al., 2014a). In addition, for Pu measurements with MC-ICP-MS, the most significant interferences are usually caused by the formation of polyatomic uranium hydrides ($^{238}\text{UH}^+$) and peak tailing from the $^{238}\text{U}^+$ peak, resulting in overestimation of the ^{239}Pu signal. The analytical procedure we employed in our work was capable of effectively eliminating the U interferences by achieving an extremely high U decontamination factor of 6.0×10^7 , which was comparable to previously reported values (3.0×10^7 – 1.0×10^8) (Bu et al., 2014a).

The data quality and the mass bias correction were assured by regular analyses of the IAEA-443 (Irish Seawater) (International Atomic Energy Agency) certified reference material ($^{240}\text{Pu}/^{239}\text{Pu} = 0.228 \pm 0.004$, $n = 18$, verified value: 0.229 ± 0.006). The analytical method was also validated by analyzing with other reference materials: IAEA-384 (Fangataufa Lagoon Sediment) and IAEA-385 (Irish Sea Sediment). The accuracies of the $^{239} + ^{240}\text{Pu}$ activities and the $^{240}\text{Pu}/^{239}\text{Pu}$ atom ratios were in good agreement with the certified and previously reported values (Table 2). In addition, the operational blank count rates for ^{239}Pu and ^{240}Pu were analyzed through measuring 100 L pure water following the same chemical procedure for Pu determination in seawater. The

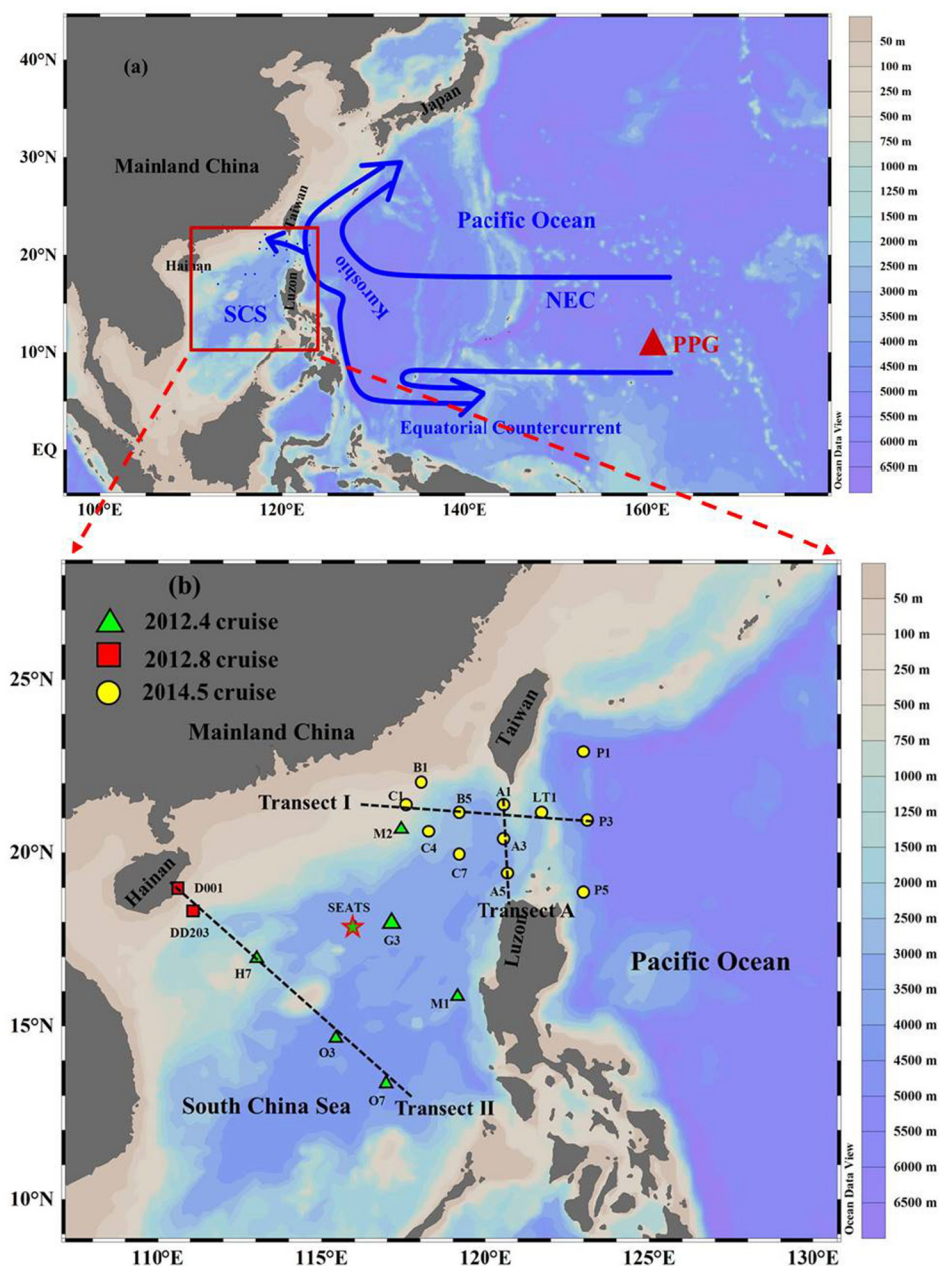


Fig. 1. Maps of the South China Sea (SCS) and the western North Pacific Ocean showing: (a) a schematic chart of the North Equatorial Current (NEC)-Kuroshio Current system, and the location of the Pacific Proving Grounds (PPG, red triangle) in the Marshall Islands (Wu et al., 2014); and (b) sampling sites in the SCS and adjacent Pacific Ocean. The range of both the NEC and Kuroshio (blue solid arrows) in the Pacific Ocean has also been roughly sketched. Green triangles and red squares represent stations where seawater samples were collected in April and August 2012, respectively; the water column was taken at the SEATS station (pentacle) in April (0–300 m, SEATS I) and August 2012 (0–1000 m, SEATS II). Yellow circles represent the sampling stations visited in May 2014. (For interpretation of the references to colour in this figure legend, the reader is referred to the web version of this article.)

limit of detection (LOD) was calculated based on the International Union of Pure and Applied Chemistry recommendations (Mocak et al., 1997). The LOD was calculated to be 0.44 fg mL^{-1} for ^{239}Pu and 0.36 fg mL^{-1} for ^{240}Pu , corresponding to 0.01 mBq m^{-3} for ^{239}Pu and 0.03 mBq m^{-3} for ^{240}Pu when a 100 L volume of water was measured.

3. Results and discussion

3.1. Hydrography

The basic hydrology of the SCS during the observation period has been introduced in Yang et al. (2016), Lin et al. (2016) and Zhong et al. (2017). Here in Fig. 2, we showed the relationship between potential temperature (θ) and (S) salinity at the sampling sites. They are

consistent with the general features reported previously (Du et al., 2013 and references therein), and have been used to differentiate them from other water masses upon mixing such as Kuroshio being indicated by data points collected at Stns P1, P3, P5 and LT1. Potential temperature and salinity were noticeably temporally variable in the surface mixed layer. For example, sea surface temperature at the SEATS station was moderately high ($\sim 28^\circ\text{C}$) in spring 2012 and increased gradually to $\sim 28.8^\circ\text{C}$ in summer 2012 (Fig. 2a). In contrast, the higher surface salinity in SEATS I was comparable to that in SEATS II, since the latter sampling period was during precipitation. Fig. 2a also underlines that the Kuroshio water influence on SEATS I was stronger compared to that on SEATS II. Below the mixed layer, the SCS water was characteristic of both a distinct shallow salinity maximum ($S > 34.6$, $\theta = \sim 18^\circ\text{C}$, $\sigma_\theta = \sim 24.8$) at about 150 m and a

Table 1
²³⁹+²⁴⁰Pu activities and ²⁴⁰Pu/²³⁹Pu atom ratios in surface seawater of the South China Sea.

Area	Station	Lat. (°N)	Long. (°E)	Bot. depth (m)	Sampling date	Layer (m)	Temperature (°C)	Salinity	²³⁹ + ²⁴⁰ Pu activities (mBq m ⁻³)	²⁴⁰ Pu/ ²³⁹ Pu atom ratios
SCS	SEATS	17.949	115.947	3833	2012-04-14	0.5	27.570	33.705	2.22 ± 0.02	0.248 ± 0.007
	M2	20.619	117.521	1289	2012-04-11	0.5	26.281	33.550	2.48 ± 0.03	0.224 ± 0.005
	M1	15.803	119.225	5133	2012-04-16	0.5	29.849	33.030	2.78 ± 0.04	0.248 ± 0.004
	H7	17.001	113.001	1628	2012-04-16	0.5	28.282	33.634	2.34 ± 0.03	0.237 ± 0.006
	O3	14.736	115.388	4360	2012-04-21	0.5	29.571	33.107	2.22 ± 0.03	0.225 ± 0.007
	O7	13.472	116.958	4270	2012-04-22	0.5	30.078	33.155	2.42 ± 0.05	0.241 ± 0.006
	G3	18.027	117.027	3874	2012-04-12	0.5	28.053	33.423	2.74 ± 0.04	0.250 ± 0.007
	SEATS	18.000	116.000	3840	2012-08-06	0.5	28.692	32.903	2.35 ± 0.04	0.242 ± 0.007
	D001	18.974	110.717	77	2012-08-14	0.5	26.995	33.492	1.80 ± 0.02	0.184 ± 0.017
	DD203	18.247	111.250	430	2012-08-16	0.5	29.841	33.260	1.59 ± 0.03	0.208 ± 0.019
Luzon Strait (Kuroshio)	A1	21.417	120.505	1685	2014-06-10	0.5	28.751	34.398	1.77 ± 0.02	0.238 ± 0.005
	A3	20.520	120.499	2109	2014-06-09	0.5	29.303	33.767	2.06 ± 0.02	0.240 ± 0.006
	A5	19.327	120.627	2170	2014-05-31	0.5	31.545	33.660	2.94 ± 0.03	0.238 ± 0.004
	B1	22.087	118.135	540	2014-06-06	0.5	28.925	32.283	2.29 ± 0.03	0.234 ± 0.005
	B5	21.202	119.258	2957	2014-06-06	0.5	30.141	34.204	2.49 ± 0.02	0.200 ± 0.005
	C1	21.280	117.586	648	2014-06-04	0.5	29.995	33.827	2.85 ± 0.03	0.220 ± 0.002
	C4	20.628	118.310	2200	2014-06-02	0.5	30.644	33.924	2.20 ± 0.03	0.246 ± 0.006
	C7	19.919	119.148	2357	2014-06-01	0.5	29.838	33.970	2.65 ± 0.03	0.240 ± 0.005
	P1	22.998	122.999	3150	2014-05-26	0.5	27.525	34.819	1.76 ± 0.02	0.255 ± 0.003
	P3	21.000	123.000	3410	2014-05-27	0.5	29.652	34.714	1.75 ± 0.02	0.250 ± 0.005
P5	19.000	123.000	3657	2014-05-29	0.5	30.726	34.506	1.64 ± 0.02	0.263 ± 0.007	
LT1	21.129	121.683	2740	2014-05-28	0.5	28.951	34.730	1.93 ± 0.02	0.251 ± 0.006	

pronounced minimum ($S = -34.4$, $\theta = -8$ °C, $\sigma_\theta = -26.8$) at approximately 400 m. The former was indicative of the North Pacific Tropical Water, while the latter represented the core of the North Pacific Intermediate Water (Chou et al., 2005). Compared to the SCS water, the higher potential temperature and salinity in Kuroshio water was observed at the same isopycnal layer. The permanent thermocline extended from the base of the mixed layer to about 1500 m. Below 1500 m, parameters such as salinity, potential temperature and potential density are almost constant at $S = -34.6$; $\theta = -2$ °C; $\sigma_\theta = -27.7$.

3.2. Spatial distribution of Pu in the SCS

3.2.1. ²⁴⁰Pu/²³⁹Pu atom ratio

The ²⁴⁰Pu/²³⁹Pu atom ratios of surface seawater in the SCS during the investigated period in 2012–2014 are presented in Table 1. They varied from 0.184 to 0.250, with an average of 0.231 ± 0.018 ($n = 18$, number of samples, thereafter). Such average levels were comparable to the previously reported values in the SCS basin (0.242 ± 0.007 , $n = 3$; Yamada et al., 2006). These ²⁴⁰Pu/²³⁹Pu atom ratios were all characteristically higher than those expected solely from the global fallout (0.178 ± 0.019 , 0–30°N) (Kelley et al., 1999), implying that this area must have received Pu from detonations of high-yield thermonuclear devices.

In the surface Kuroshio water, even higher ²⁴⁰Pu/²³⁹Pu atom ratios than in the SCS were observed, varying from 0.250 to 0.263, with an

average of 0.255 ± 0.006 ($n = 4$), which apparently fueled the high ²⁴⁰Pu/²³⁹Pu atom ratio signal in the SCS along with the intrusion of the Kuroshio. This can also be clearly seen from Fig. 2b, showing that the ²⁴⁰Pu/²³⁹Pu atom ratios decreased from the Kuroshio to the SCS along the isopycnal surface. Such an influence from the Kuroshio can also be seen from the small difference in ²⁴⁰Pu/²³⁹Pu atom ratio in spring when the Kuroshio has more impact on the SEATS station than in summer. Indeed a slightly but visibly elevated ratio occurred in spring (0.248 ± 0.007) compared to summer (0.242 ± 0.007). Within the SCS, the distribution of ²⁴⁰Pu/²³⁹Pu atom ratios also showed a decreasing trend away from the Luzon Strait, very consistent with the introduction pathway of the Kuroshio Current into the SCS (Fig. 3a).

The depth profiles of the ²⁴⁰Pu/²³⁹Pu atom ratio along with temperature (T) and salinity (S) at the SEATS station are presented in Fig. 4. The ²⁴⁰Pu/²³⁹Pu atom ratio at SEATS I ranged from 0.216–0.248 (Table 3). Similar results were obtained from the SEATS II water column, where the ²⁴⁰Pu/²³⁹Pu atom ratio was 0.217–0.242 in the upper 1000 m. The range of the ²⁴⁰Pu/²³⁹Pu atom ratios in the water column from the SCS agreed well with those in the sediment cores from the NSCS shelf (Wu et al., 2014) with significantly higher values than the global fallout (Kelley et al., 1999).

The depth profile of ²⁴⁰Pu/²³⁹Pu atom ratio of SEATS I showed a decreasing trend from 0.248 at the surface to 0.216–0.222 at 100–200 m (Fig. 4a). For SEATS II, we sampled through the upper 1000 m showing again a decrease from 0.242 at the surface to 0.217 at 200 m, followed by

Table 2
 Analytical results of ²³⁹+²⁴⁰Pu activities and ²⁴⁰Pu/²³⁹Pu atom ratios in the reference materials.

Reference materials	Measured ²³⁹ + ²⁴⁰ Pu activity (mBq)	Added ²³⁹ + ²⁴⁰ Pu activity (mBq)	Measured ²⁴⁰ Pu/ ²³⁹ Pu atom ratio	²⁴⁰ Pu/ ²³⁹ Pu information values	Accuracy ^b	Precision	Reference
IAEA-443 ^a	2.96 ± 0.05 (n = 18)	2.90–3.04	0.228 ± 0.004 (n = 18)	0.229 ± 0.006	0.3% (activity) 0.4% (ratio)	1.6% (activity) 1.8% (ratio)	Pham et al., 2011
Reference materials	Measured ²³⁹ + ²⁴⁰ Pu activity (mBq g ⁻¹)	Certified ²³⁹ + ²⁴⁰ Pu activity (mBq g ⁻¹)	Measured ²⁴⁰ Pu/ ²³⁹ Pu atom ratio	²⁴⁰ Pu/ ²³⁹ Pu literature values	Accuracy	Precision	Reference
IAEA-384	109.07 ± 3.12 (n = 5)	107 (103–110)	0.052 ± 0.001 (n = 5)	0.045–0.053 (n = 9)	1.9% (activity)	2.9% (activity) 1.9% (ratio)	Povinec et al., 2007; Lindahl et al., 2010, 2011; Godoy et al., 2009
IAEA-385	2.96 ± 0.04 (n = 3)	2.96 (2.89–3.00)	0.184 ± 0.003 (n = 3)	0.178–0.192 (n = 3)	0% (activity)	1.4% (activity) 1.6% (ratio)	Lindahl et al., 2010; Pham et al., 2008

Uncertainties of the data are ± 1σ based on counting statistics and standard propagation of errors.

^a About 202.7 g IAEA-443 (14.3–15.0 mBq kg⁻¹) was added into ~100 L water.

^b The percent represents the accuracy and precision of the ²³⁹+²⁴⁰Pu activity and ²⁴⁰Pu/²³⁹Pu atom ratio, respectively.

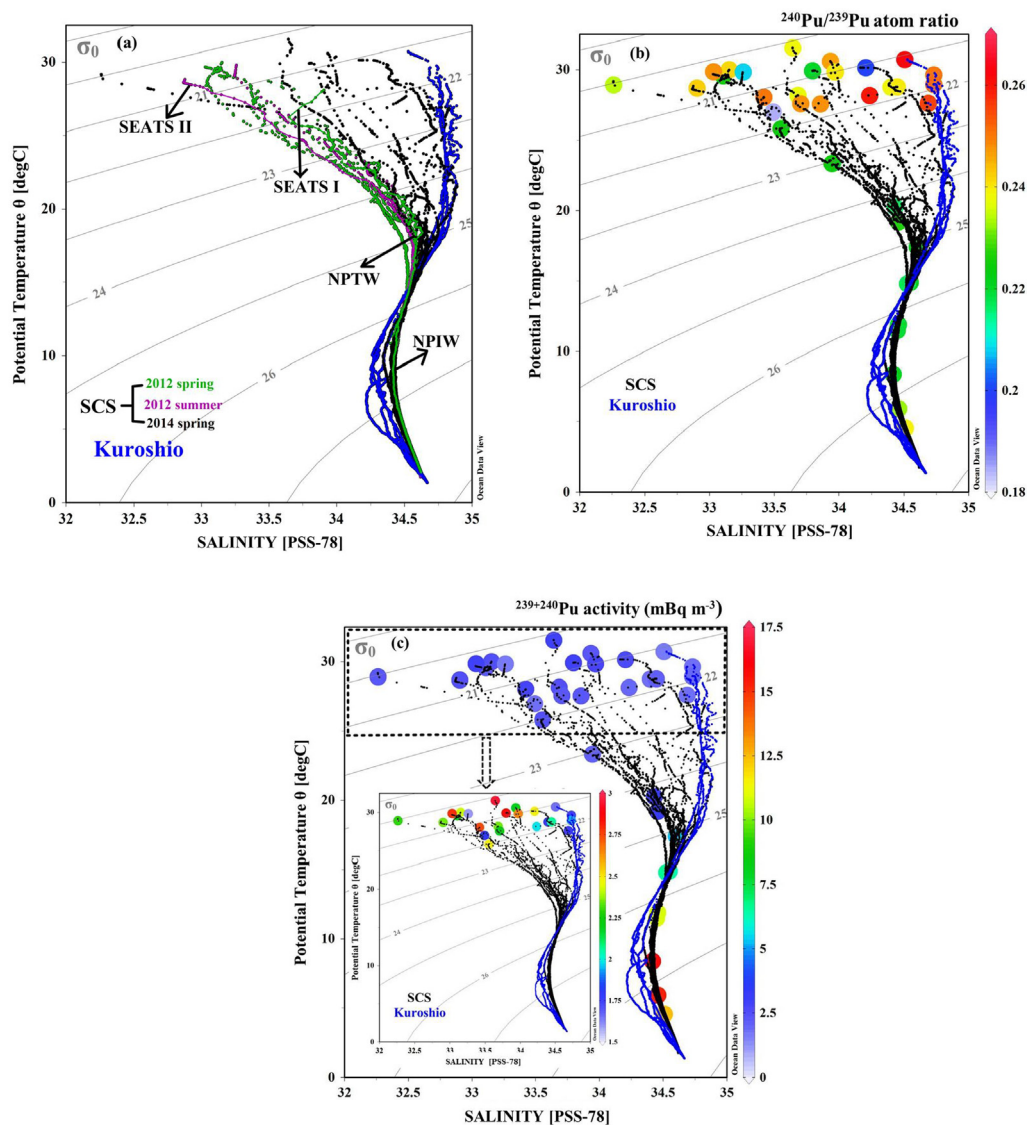


Fig. 2. (a) Potential temperature (θ) versus salinity (S) plots ($\theta - S$ diagram) in the water column for the sampling station in the central South China Sea (SCS) during 2012–2014. The Kuroshio water is represented by Stns P1, P3, P5 and LT1. Here, NPTW denotes North Pacific Tropical Water, and NPIW denotes North Pacific Intermediate Water. (b) $\theta - S$ diagram superimposed with the $^{240}\text{Pu}/^{239}\text{Pu}$ atom ratio. (c) $\theta - S$ diagram superimposed with the $^{239} + ^{240}\text{Pu}$ activity (unit: mBq m^{-3}). Temperature and salinity data in spring, summer 2012 and spring 2014 were cited from Yang et al. (2016), Lin et al. (2016) and Zhong et al. (2017), respectively.

a more gradual increase to 1000 m, reaching 0.239 (Fig. 4b). The high $^{240}\text{Pu}/^{239}\text{Pu}$ atom ratio in the surface should be related to the Pu sourced from the Kuroshio intrusion with a higher $^{240}\text{Pu}/^{239}\text{Pu}$ atom ratio as shown above. The Kuroshio intrusion is mostly limited to the upper 100–200 m resulting where a minimum of $^{240}\text{Pu}/^{239}\text{Pu}$ atom ratio was observed. This close-in fallout fraction with higher $^{240}\text{Pu}/^{239}\text{Pu}$ atom ratio was characterized by large size particles and could be preferentially scavenged from the water column (Buesseler, 1997), resulting in declines in Pu atom ratios in the upper 100–200 m (see later discussion). The increase beyond the upper water column should be attributable to the remineralization of biogenic particle packaged Pu, which released the close-in fallout Pu back to the water column. Indeed, remineralization of the particle packaged nitrogen isotope (Wong et al., 2002) and ^{234}Th (Wei et al., 2011) in the SCS were also observed beyond 100–200 m.

3.2.2. $^{239} + ^{240}\text{Pu}$ activity

The $^{239} + ^{240}\text{Pu}$ activities in the SCS surface seawater during the period of investigation are also listed in Table 1. They ranged from 1.59 to 2.94 mBq m^{-3} , with an average of $2.34 \pm 0.38 \text{ mBq m}^{-3}$ ($n = 18$). Such

$^{239} + ^{240}\text{Pu}$ activity levels were slightly lower than the previously reported values in the SCS basin ($2.51 \pm 0.21 \text{ mBq m}^{-3}$, $n = 3$; Yamada et al., 2006). The distribution of $^{239} + ^{240}\text{Pu}$ in the SCS surface seawater overall showed an increasing trend from the Luzon Strait to the basin, followed by a decrease from the basin towards the shelf (Fig. 3b). For example, the $^{239} + ^{240}\text{Pu}$ activities along transect I (Stns P3, LT1, B5, C1) increased from 1.75 mBq m^{-3} (Stn. P3) to 2.85 mBq m^{-3} (Stn. C1), while along transect II (Stns O7, O3, H7, DD203, D001) they decreased from 2.42 mBq m^{-3} (Stn. O7) to 1.80 mBq m^{-3} (Stn. D001).

In the surface Kuroshio water, the $^{239} + ^{240}\text{Pu}$ activities varied from 1.64 to 1.93 mBq m^{-3} , with an average of $1.77 \pm 0.12 \text{ mBq m}^{-3}$ ($n = 4$), which were $\sim 40\%$ lower than that in the SCS basin. Fig. 2c also underlines an increase in $^{239} + ^{240}\text{Pu}$ activities along the isopycnal surface from the Kuroshio to the SCS. Such influences from the Kuroshio can also be seen from the small difference in $^{239} + ^{240}\text{Pu}$ activity between in spring when the Kuroshio has more impact at the SEATS station than in summer. Indeed, slightly but visible lower activity occurred in spring (2.22 ± 0.02) than in summer (2.35 ± 0.04).

The $^{239} + ^{240}\text{Pu}$ activities in the water column of SEATS I ranged from 2.07 to 10.96 mBq m^{-3} , and those of SEATS II varied from 2.35 to

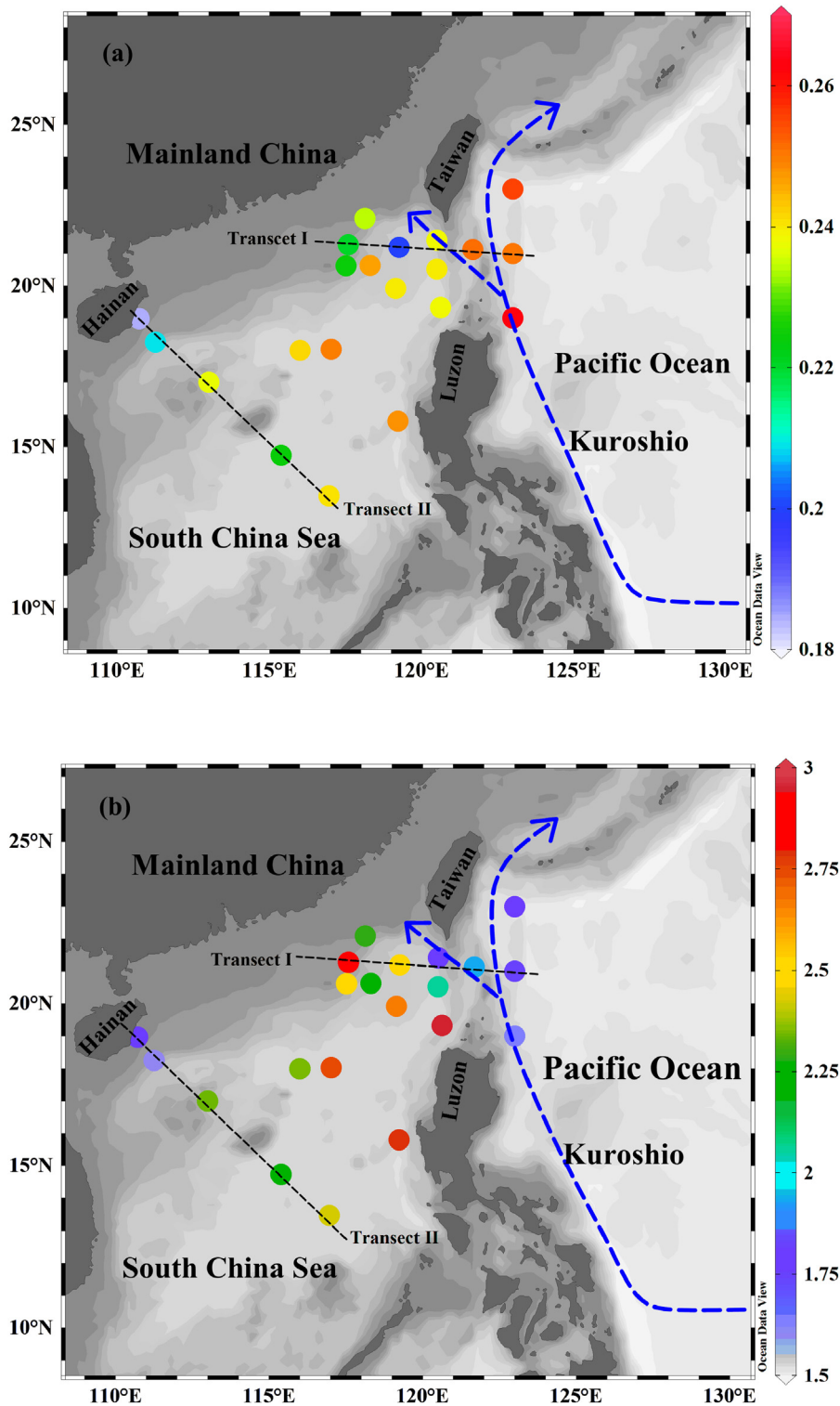


Fig. 3. Distributions of (a) $^{240}\text{Pu}/^{239}\text{Pu}$ atom ratio; and (b) $^{239} + ^{240}\text{Pu}$ activity (unit: mBq m^{-3}) in the surface seawater of the South China Sea and across the Luzon Strait.

15.69 mBq m^{-3} . The profile of $^{239} + ^{240}\text{Pu}$ activities showed an increasing trend with depth and a pronounced sub-surface maximum centered at 500 m, followed by a more gradual decline (Fig. 4b). Such a pattern was generally consistent with those observed in other oceanic regimes (Bowen et al., 1980; Tsumune et al., 2003), showing a broad maximum over the depth interval 500–1000 m in the Japan Sea (Hirose et al., 1999; Ito et al., 2003; Lee et al., 2003) and 300–800 m in the Pacific Ocean (Bowen et al., 1980; Kinoshita et al., 2011; Yamada and Zheng, 2012). Based on the θ –S diagram illustrated in Fig. 2a, SEATS II was

primarily of SCS water mass with little influence from the Kuroshio intrusion in the upper 400 m. The maximum $^{239} + ^{240}\text{Pu}$ activity appeared at 500 m and as shown in Fig. 4b was located at the SCS intermediate water where net outflow into the wNPO occurred. Note that we are not entirely certain about the maxima Pu depth owing to the coarse sampling resolution at depths. Nevertheless, the maximum $^{239} + ^{240}\text{Pu}$ activity at the SCS intermediate layer suggested that the high activity must be a result of difference in vertical particle scavenging across this depth horizon, i.e., higher scavenging above and lower below. Indeed,

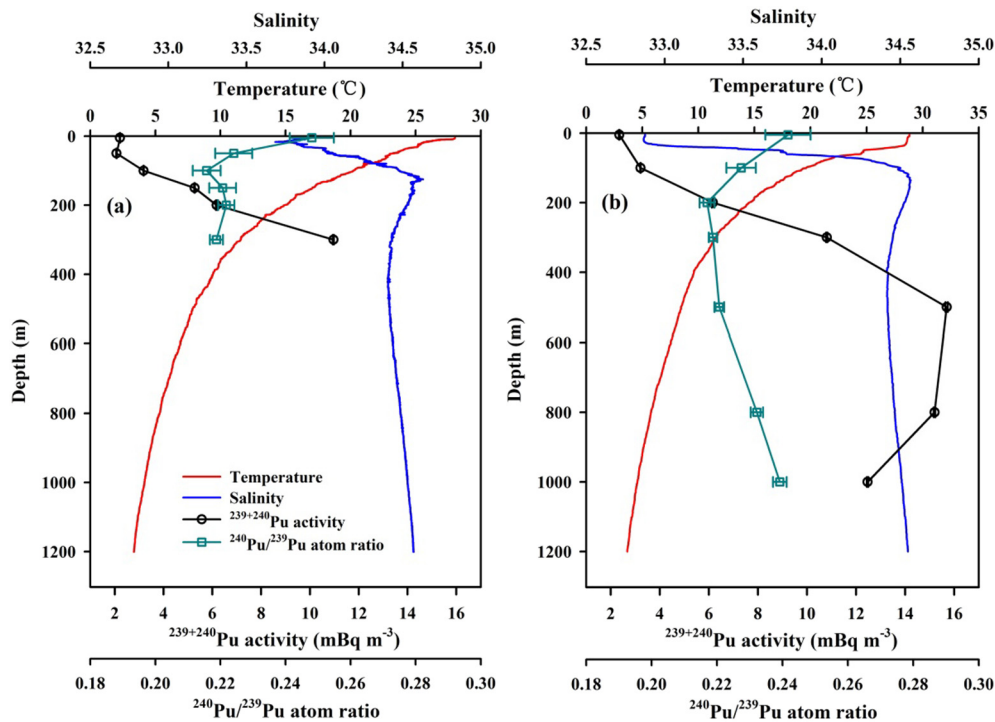


Fig. 4. Vertical profiles of $^{239} + ^{240}\text{Pu}$ activity, $^{240}\text{Pu}/^{239}\text{Pu}$ atom ratio and temperature-salinity at the SEATS stations in (a) April 2012; and (b) August 2012 in the South China Sea.

it was seen that total suspended matter (TSM) from the shelf through lateral transport was visible at this depth range of the upper 300 m (Fig. 5), which would enhance the scavenging. Beyond 400–500 m, TSM stayed low, and regeneration as a result of microbial decomposition of particles during the downward transport should be dominant. This lateral transport of shelf-origin material is in fact commonly observed in the SCS (Liu et al., 2014; Schroeder et al., 2015; Liu et al., 2016) and elsewhere such as in the North Atlantic Ocean (Falkowski et al., 1994).

3.3. Scavenging and accumulation of Pu

3.3.1. Scavenging of Pu

We have shown significant vertical gradients in $^{240}\text{Pu}/^{239}\text{Pu}$ atom ratio at the SEATS station which would have been uniform if the source term was solely from the global fallout. Such fractionation cannot be induced by biological activity, and thus they are attributable to the different source functions and different scavenging efficiency between differently sourced Pu. As presented above with respect to the spatial distribution, Pu transported by the Kuroshio was an obvious source

term, traceable to the PPG presenting two main source terms of Pu, namely global fallout and close-in fallout transported via currents. Within the SCS water column, the vertical difference in $^{240}\text{Pu}/^{239}\text{Pu}$ atom ratio would be subsequently determined by the different scavenging efficiency of different Pu particles.

It is well known that the physical and/or chemical form of Pu-bearing particles is different depending on testing conditions (Buesseler, 1997). Global fallout particles originate directly from the vaporization and condensation of nuclear weapons materials and are characterized by their sub-micron size, typically at 0.1–1.0 μm in size (Adams et al., 1960; Joseph et al., 1971; Weimer and Langford, 1978). Pu associated with these small particles is thus by nature less efficiently scavenged, or has a longer residence time in the seawater. In contrast, the close-in fallout typically incorporates large quantities of partially and completely vaporized calcium, carbonates, calcium oxides and calcium hydroxides (typically >1.0 μm in size) (Adams et al., 1960; Joseph et al., 1971). The Pu attached to the relatively larger particles such as calcium hydroxides is thus by nature more efficiently scavenged, or has a shorter residence time in the seawater. As a matter of fact, higher $^{240}\text{Pu}/^{239}\text{Pu}$ ratios in the water column have been found in

Table 3
 $^{239} + ^{240}\text{Pu}$ activities and $^{240}\text{Pu}/^{239}\text{Pu}$ atom ratios in the water column from the South China Sea.

Sample	Lat. (°N)	Long. (°E)	Bot. depth (m)	Sampling date	Layer (m)	Temperature (°C)	Salinity	$^{239} + ^{240}\text{Pu}$ activities (mBq m ⁻³)	$^{240}\text{Pu}/^{239}\text{Pu}$ atom ratio
SEATS I	17.949	115.947	3833	2012-04-14	0.5	27.570	33.705	2.22 ± 0.02	0.248 ± 0.007
					50	23.323	34.029	2.07 ± 0.02	0.224 ± 0.006
					100	22.220	34.478	3.19 ± 0.03	0.216 ± 0.004
					150	17.060	34.559	5.27 ± 0.05	0.221 ± 0.004
					200	14.922	34.528	6.18 ± 0.12	0.222 ± 0.003
					300	11.556	34.432	10.96 ± 0.22	0.219 ± 0.002
SEATS II	18.000	116.000	3840	2012-08-06	0.5	28.692	32.903	2.35 ± 0.05	0.242 ± 0.007
					100	19.582	34.501	3.22 ± 0.03	0.227 ± 0.005
					200	14.503	34.525	6.17 ± 0.25	0.217 ± 0.002
					300	11.516	34.453	10.81 ± 0.32	0.219 ± 0.001
					500	8.466	34.419	15.69 ± 0.78	0.221 ± 0.002
					800	5.778	34.466	15.20 ± 0.46	0.232 ± 0.002
					1000	4.574	34.510	12.47 ± 0.37	0.239 ± 0.002

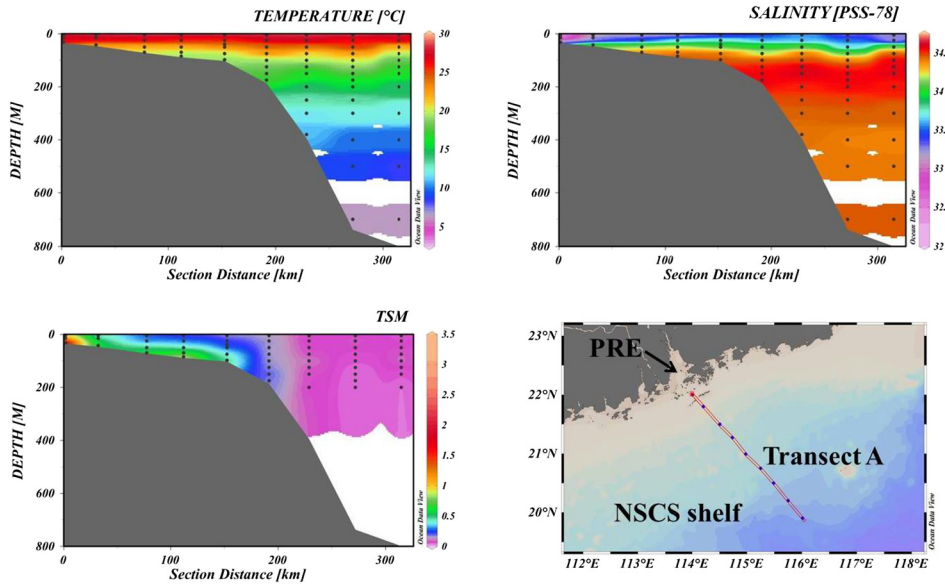


Fig. 5. Vertical distribution of temperature, salinity and total suspended matter (TSM) (mg L^{-1}) along Transect A on the NSCS shelf in August 2012.

other marginal seas of the Western Pacific impacted by the Kuroshio. In the East China Sea, $^{240}\text{Pu}/^{239}\text{Pu}$ atom ratios are 0.234 ± 0.012 ($n = 7$; Yamada and Zheng, 2011). In the Japan Sea, $^{240}\text{Pu}/^{239}\text{Pu}$ atom ratios are 0.240 ± 0.010 ($n = 43$; Kim et al., 2004; Yamada and Zheng, 2010). Moreover, the average $^{240}\text{Pu}/^{239}\text{Pu}$ atom ratio in the surface seawater (0.231 ± 0.018 , $n = 18$) is significantly lower than that of surface sediments (0.268 ± 0.010 , $n = 18$; Wu et al., 2014), further confirming that the Pu originating from non-global fallout was more rapidly removed from the water column and was preferentially accumulated in the sediments.

The $^{239} + ^{240}\text{Pu}$ inventory can further help in deciphering the removal efficiency and lateral transport of Pu in both dissolved and particulate forms (Bowen et al., 1980; Buesseler, 1997). In our study, we calculated the $^{239} + ^{240}\text{Pu}$ inventory in the water column by interpolating the activity of the $^{239} + ^{240}\text{Pu}$ at each depth (Ito et al., 2003). The $^{239} + ^{240}\text{Pu}$ inventory of the SEATS II water column from surface to 1000 m was estimated to be $11.7 \pm 0.4 \text{ Bq m}^{-2}$. This value was comparable to that of the Pacific Ocean at the same integral water depth (0–1000 m) (Table 4) (Kinoshita et al., 2011; Yamada and Zheng, 2012). Note, however, that the estimated $^{239} + ^{240}\text{Pu}$ inventory represented only a part of the whole water column because we only sampled 0–1000 m. We thus carefully examined the literature data concerning the profiles of the

$^{239} + ^{240}\text{Pu}$ activity in the Pacific Ocean and found that the spatial variation is not that big where the typical percentage of the $^{239} + ^{240}\text{Pu}$ inventory at a depth interval of 0–1000 m accounted for the whole water column is in the range of 31.0–48.5%, with an average of 40.6% ($n = 12$) (Kinoshita et al., 2011; Yamada and Zheng, 2012). Given that the depth profiles in the SCS in the upper 1000 m were rather similar to that in the Pacific, we extrapolated our upper 1000 m inventory to the whole water column using the percentage partitioning in the Pacific Ocean. Thus, the $^{239} + ^{240}\text{Pu}$ inventory of the whole water column at the SEATS station was roughly estimated to be 29 Bq m^{-2} ($24\text{--}38 \text{ Bq m}^{-2}$), which was compared to that expected from global fallout at the same latitudinal belts of 10–20°N ($\sim 22.2 \text{ Bq m}^{-2}$) (UNSCEAR, 2000). We point out that this estimation was subject to uncertainty. We then compared this $^{239} + ^{240}\text{Pu}$ inventory with the sediment cores obtained in the NSCS shelf (Wu et al., 2014) and the SCS basin (Dong et al., 2010), and found the following two features (Fig. 6): 1) the $^{239} + ^{240}\text{Pu}$ inventory of the water column in the SCS basin was significantly lower than that of the sediment core in the NSCS shelf; and 2) in the SCS basin, the $^{239} + ^{240}\text{Pu}$ inventory of the water column was higher than that in the sediment core. The difference in the $^{239} + ^{240}\text{Pu}$ inventory between the water column and the sediment core was caused by the difference in Pu scavenging efficiency.

Table 4
Estimated $^{239} + ^{240}\text{Pu}$ inventories in the South China Sea and in other oceanic settings.

Area	Stations	Locations (Lat., Long.)	Sampling date (yyyy-mm)	Integral depth (m)	$^{239} + ^{240}\text{Pu}$ inventory (Bq m^{-2})	$^{239} + ^{240}\text{Pu}$ percentage at 0–1000 m ^a	References
SCS	SEATS	18.0°N, 116.0°E	2012-08	0–1000	11.7 ± 0.4	40.6	This study
Equatorial Pacific Ocean	AQ-7	0.0°N, 178.9°E	1990-11	0–1000	9.6	34.0	Yamada and Zheng, 2012
	AQ-13	5.0°S, 168.9°E	1990-11	0–1000	8.0	37.9	
Tropical East Pacific Ocean	HY-1	20.0°N, 140.0°W	2003-06	0–1000	16.2 ± 0.6	43.7 ± 1.8	Kinoshita et al., 2011
	HY-2	16.5°N, 123.0°W	2003-07	0–1000	24.8 ± 0.7	48.5 ± 1.8	
	HY-3	8.0°N, 95.5°W	2003-07	0–1000	21.4 ± 0.6	42.7 ± 1.4	
	HY-6	0.0°N, 95.5°W	2003-07	0–1000	20.2 ± 0.5	42.9 ± 1.1	
	HY-9	8.0°S, 95.0°W	2003-07	0–1000	12.9 ± 0.4	33.1 ± 1.2	
	HY-11	15.0°S, 85.8°W	2003-07	0–1000	7.9 ± 0.2	31.0 ± 0.9	
	HY-12	20.0°S, 101.0°W	2003-07	0–1000	5.5 ± 0.1	45.4 ± 1.7	
	HY-15	25.0°S, 116.0°W	2003-08	0–1000	3.6 ± 0.1	45.9 ± 2.3	
	HY-17	28.5°S, 127.8°W	2003-08	0–1000	4.6 ± 0.2	42.5 ± 1.6	
	HY-18	26.0°S, 140.0°W	2003-08	0–1000	4.8 ± 0.1	39.2 ± 1.2	

^a The values represent the percentage of $^{239} + ^{240}\text{Pu}$ inventory at 0–1000 m accounting for the whole water column and the SCS value is taken from the averages of literature on the Pacific Ocean.

The removal efficiency in the water column is largely related to water depth and particle abundance. The water depths at the locations where we collected samples on the shelf were much shallower than those of the SCS basin, so the residence time of Pu in the water column was much shorter over the nearshore than over the deep SCS basin. Obviously, the abundant terrestrial input of nutrients and the China Coastal Current lead to elevated biological productivity and particle fluxes (Han et al., 2012), facilitating the scavenging of Pu from the water column on the shelf (Sholkovitz, 1983; McCubbin et al., 2004). In contrast, the greater water depth of the SCS basin leads to lower supply and longer transit time from the water column to the sediment. Longer residence time of suspended particles in the deep SCS is obviously favorable for the remineralization of their biogenic components and hence the recycling of Pu isotopes during the downward deposition and scavenging processes. Therefore, the $^{239} + ^{240}\text{Pu}$ of the water column was more easily and quickly scavenged than the sediment on the shelf, while for the deep ocean basin, much of the $^{239} + ^{240}\text{Pu}$ would still be preserved in the water column. The Pu scavenging efficiency in the NSCS shelf was higher than that in the SCS basin. Indeed, the data sets of another particle reactive radionuclide similar to $^{239} + ^{240}\text{Pu}$, ^{234}Th in the SCS published elsewhere (Cai et al., 2015), also support this viewpoint. ^{234}Th exhibits a larger deficit in the NSCS shelf compared to the SCS basin, and the scavenging efficiency of ^{234}Th at Stn. A7 (close to the investigated Stn. A8) is about six times (four to eight times) that of the SEASTS station (Cai et al., 2015). Under the assumption that the $^{239} + ^{240}\text{Pu}$ inventory of sediment was derived mainly from the Pu scavenged from the water column and as a first order of estimation, we calculated that the scavenging efficiency of $^{239} + ^{240}\text{Pu}$ in the SCS basin was ~11.6% (9.1–13.6%), comparable to that of ^{234}Th (~10.8%) (Cai et al., 2015). In contrast, the scavenging efficiency of $^{239} + ^{240}\text{Pu}$ in the NSCS shelf water column was estimated to be ~69.6% (36.4–92.8%), compared to the similar estimation of ^{234}Th in this region (~60.7%) (Cai et al., 2015). It is worth noting that these estimates are subject to large uncertainty due to limited field data points.

3.3.2. Accumulation of Pu

The fact that the $^{239} + ^{240}\text{Pu}$ activity levels in the SCS basin were significantly higher than those in the Kuroshio water suggests accumulation of Pu in the SCS. This accumulation was likely due to the fast scavenging of non-global fallout. Actually, the Kuroshio water is featured by even lower nutrients, biological productivity and TSM compared to the SCS seawater (Wong et al., 2000; Du et al., 2013; Wu et al., 2015), and so Pu in the SCS would have been more readily removed from the water column if the global fallout was the only source

in both systems, which was obviously not the case. The accumulation of Pu in the SCS would thus imply that the difference in scavenging efficiency between the SCS and Kuroshio was not the major driving factor determining the difference between them. We suggest that the lower $^{239} + ^{240}\text{Pu}$ activity of the Kuroshio was mainly associated with a unique close-in fallout source with high $^{240}\text{Pu}/^{239}\text{Pu}$ atom ratio which has already been subject to high degrees of scavenging on the pathway to the Kuroshio. Apparently, this high $^{240}\text{Pu}/^{239}\text{Pu}$ atom ratio can be traced back to the Kuroshio precursor, the NEC originating approximately from the PPG. The Eniwetok and Bikini Atolls are located within the NEC and large-scale USA nuclear tests conducted at the PPG in the 1950s released a substantial radioactive fallout yield (Bowen et al., 1980; Buesseler, 1997) which may have been transported westward following the NEC and fed into its northward bifurcation-Kuroshio Current off the Philippines. This high $^{240}\text{Pu}/^{239}\text{Pu}$ “stream” along the NEC-Kuroshio is evident when compared with the $^{240}\text{Pu}/^{239}\text{Pu}$ atom ratios beyond this pathway in the WNPO (0.207 ± 0.010 , $n = 4$) (Yamada et al., 2006) and its adjacent marginal seas, such as in the Sulu and Indonesian Seas, where $^{240}\text{Pu}/^{239}\text{Pu}$ atom ratios are 0.237 ± 0.007 ($n = 4$; Yamada et al., 2006), and in the Japan Sea, where $^{240}\text{Pu}/^{239}\text{Pu}$ atom ratios are 0.240 ± 0.010 ($n = 24$; Kang et al., 1997; Hirose et al., 1999, 2002; Yamada and Zheng, 2008). The supply of Pu from the PPG via the NEC-Kuroshio into the SCS appeared to be continuous as evidenced by the persistent high $^{240}\text{Pu}/^{239}\text{Pu}$ atom ratio observed in the SCS at present, 60 years since the nuclear tests were banned on the Marshall Islands. The continuous release of Pu at the PPG transported towards the Indian Ocean is reported by Pittauer et al. (2017). As a consequence, the close-in fallout carried by the Kuroshio from the PPG evolved and is characterized by low $^{239} + ^{240}\text{Pu}$ activity and high $^{240}\text{Pu}/^{239}\text{Pu}$ atom ratio at present.

The residence time of upper Kuroshio water (0–500 m) off the Luzon Strait is estimated as 8.3 days (5.3–19.3 days) under the assumption of a constant transport velocity (Centurioni et al., 2004). This is substantially lower than that of upper seawater in the SCS (~3.1–5.7 years, with an average of ~3.9 years) (Qu et al., 2006). The longer residence time in the SCS obviously facilitated the accumulation of Pu in the water column.

We now know that the Pu from the PPG is responsible for the high $^{239} + ^{240}\text{Pu}$ activity in the SCS because of long-term accumulation. Indeed, high $^{239} + ^{240}\text{Pu}$ activity in the sediment core of the NSCS shelf is also recorded corresponding to this period (Wu et al., 2014). Similarly, compared to the Kuroshio, enhanced $^{239} + ^{240}\text{Pu}$ activities in other marginal seas of the Western Pacific such as the Sulu and Indonesian Seas (Yamada et al., 2006) and the Japan Sea (Kang et al., 1997; Hirose et al., 1999, 2002; Yamada and Zheng, 2008) may suggest that such accumulation is ubiquitous.

3.4. Semi-quantitative estimation of the PPG contribution

While the PPG has proven to be a continuous Pu source term, we should also examine other possible sources to the SCS including nuclear accidents (Chernobyl and Fukushima), on-going nuclear power plants and other local fallout. Kim et al. (2004) confirm that the contribution of Chernobyl-derived Pu is negligible in the marginal seas of the North Pacific Ocean. Our sediment work in the NSCS shelf suggests there is no Pu signature from the Fukushima nuclear accident (Wu et al., 2014). There are two nuclear power plants (Daya Bay and Ling Ao located in Shenzhen) which have been operating since 1994 and 2003, respectively. However, all Pu produced in the reactors are confined within the fuel elements and there is no report of the leakage of nuclear fuel, and hence the Pu contribution would also be negligible. The $^{240}\text{Pu}/^{239}\text{Pu}$ atom ratios (~0.18) in Chinese profile soils reveal that the direct input from the close-in fallout from Lop Nor and Semipalatinsk nuclear tests did not lead to any significant Pu contribution in these areas (Zheng et al., 2009; Bu et al., 2014c), in view of their distinctive $^{240}\text{Pu}/^{239}\text{Pu}$ atom ratios of <0.1 (Wu et al., 2010) and 0.03–0.05 (Beasley et al., 1998), respectively. Considering the fact that the SCS

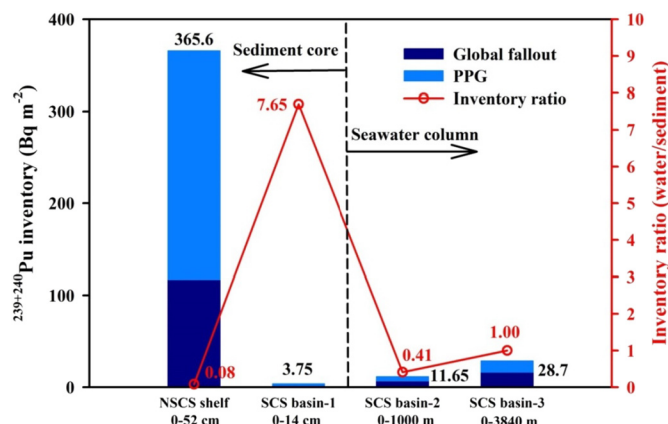


Fig. 6. $^{239} + ^{240}\text{Pu}$ inventories of the water column and sediment cores in the South China Sea and their inventory ratios (water column/sediment core). The blue and azure columns represent the contributions of global fallout and the PPG. The $^{239} + ^{240}\text{Pu}$ inventories of the sediment cores were derived from previous studies (Dong et al., 2010; Wu et al., 2014). (For interpretation of the references to colour in this figure legend, the reader is referred to the web version of this article.)

location and the catchment of the rivers flowing into the SCS is far from the sites of Lop Nor and Semipalatinsk nuclear tests site, their Pu contribution appears to be negligible. Indeed, the distribution of $^{240}\text{Pu}/^{239}\text{Pu}$ atom ratios in the NSCS shelf and PRE sediment show a landward decrease from the outer shelf consistent with the introduction of Kuroshio water (Wu et al., 2014). The $^{240}\text{Pu}/^{239}\text{Pu}$ atom ratios within a ~75 km radius off the PRE outlet are mainly from the contribution of global fallout (Wu et al., 2014), further indicating that the Pu signature from land input reached only this area. Here, we further confirmed that Pu from the PPG was a sole non-global fallout source in the SCS. Therefore, the Pu in the SCS is sourced both from global fallout and close-in fallout from the PPG, the latter being continuously supplied to the SCS via the NEC and the Kuroshio Current. We could then estimate the relative contribution from the PPG to the SCS using a two end-member mixing model.

Two stages of the process should be considered: 1) the contribution from the PPG to the Kuroshio, which depends on the dilution effect and, 2) the contribution from the Kuroshio to the SCS when they are exchanged via the Luzon Strait. First, we employed a two end-member mixing model to estimate the contribution from the PPG to the Kuroshio (Krey, 1976; Wu et al., 2014), and the estimated result showed that the average contribution from the PPG to the Kuroshio was $57 \pm 16\%$ ($n = 4$). Secondly, in order to estimate the contribution from the Kuroshio to the SCS when they are exchanged via the Luzon Strait, we hypothesized that the Pu source in the SCS from the Kuroshio be considered as a secondary source as a substitute for the PPG. This was in consideration of their exchange time being significantly shorter than the transit time of surface seawater masses from the PPG to the SCS (Wu et al., 2014), and employed another two end-member isopycnal mixing model and defined the following equation:

$$(Pu)_S = \theta * (Pu)_K + (1-\theta) * (Pu)_G \quad (1)$$

where (Pu) and θ represent the $^{239} + ^{240}\text{Pu}$ activity and the fractional contributions of the Kuroshio water when mixing had occurred between the Kuroshio water and the SCS water proper along the isopycnal surface. The subscripts K , G and S refer to the Kuroshio, global fallout and the SCS; and the partitioning between $(Pu)_K$ and $(Pu)_G$ is defined by the following equation:

$$Y = \frac{(Pu)_K}{(Pu)_G} \quad (2)$$

Based on mass balance, we deduced Eq. (3) from Eqs. (1) and (2) as:

$$Y = \frac{(Pu)_K}{(Pu)_G} = \frac{(1-\theta)(R_G - R_S)(1 + 3.674R_K)}{\theta(R_S - R_K)(1 + 3.674R_G)} \quad (3)$$

while the relative contribution in the SCS from the Kuroshio (f_k) can also be expressed as:

$$f_k = \frac{\theta(Pu)_K}{(Pu)_S} = \frac{\theta Y}{\theta(Y-1) + 1} \quad (4)$$

where R represents the $^{240}\text{Pu}/^{239}\text{Pu}$ atom ratio, and the coefficient 3.674 is a factor used to convert between the activity ratio and atom ratio of $^{240}\text{Pu}/^{239}\text{Pu}$. In the calculation, R_S was the $^{240}\text{Pu}/^{239}\text{Pu}$ atom ratio in the SCS, R_G was taken to be 0.178 ± 0.019 at the latitudinal belts of 0–30°N (Kelley et al., 1999) and R_K was 0.255 ± 0.006 ($n = 4$). The calculated methodology of θ is illustrated in a previous study (Du et al., 2013). The calculated results showed that the contribution to the SCS from the Kuroshio ranged from 9 to 94%, with an average contribution of $72 \pm 23\%$ ($n = 19$). Finally, we synthesized the two stages of the process and semi-quantitatively estimated that the PPG contribution to the SCS ranged from 5 to 54%, with an average contribution of $41 \pm 17\%$ ($n = 18$). According to Bowen et al. (1980), the total sediment inventory of $^{239} + ^{240}\text{Pu}$ is $\sim 9.62 \times 10^{13}$ Bq at the Marshall Islands while the export

flux to the Pacific Ocean is $\sim 2.22 \times 10^{11}$ Bq year $^{-1}$ by remobilizing Pu deposited in the lagoons and surrounding sediments (Noshkin et al., 1987). We thus estimated the total $^{239} + ^{240}\text{Pu}$ of the surface seawater (down to upper mixed layer depth, MLD) from the PPG to be $\sim 9.1 \times 10^{10}$ Bq. Meanwhile, the total $^{239} + ^{240}\text{Pu}$ of the surface seawater (MLD = 20–100 m: Kao et al., 2012) was also estimated to be $\sim 20.5 \times 10^{10}$ Bq ($\sim 16.4 \times 10^{10}$ – 81.9×10^{10} Bq) based on our field observation, further calculating the PPG contribution as $\sim 44\%$ (~ 11 – 56%), which was well coupled with the results estimated using the two end-member isopycnal mixing model. In addition, the distribution of the PPG contribution to the SCS is plotted in Fig. 7 and shows that the PPG contribution gradually decreased along the introduction route of the Kuroshio into the SCS from the Luzon Strait to the nearshore area, and had a large spatial variation. For example, the contribution from the PPG in the SCS basin ($\sim 45 \pm 13\%$) was about threefold that of the nearshore areas ($\sim 15 \pm 5\%$). The estimated results were also comparable to previous similar estimates made for the SCS basin ($\sim 42\%$, $n = 3$) and the Sulu Sea ($\sim 39\%$, $n = 4$) from limited data sets (Yamada et al., 2006), but significantly lower than the sediment estimates made for the NSCS shelf ($\sim 68\%$, $n = 18$: Wu et al., 2014) and SCS basin ($\sim 57\%$, $n = 1$: Dong et al., 2010).

4. Conclusions

The $^{239} + ^{240}\text{Pu}$ activities in the SCS surface seawater were slightly lower than those in the other adjacent marginal seas such as the Sulu and Indonesian Seas (3.16 ± 0.32 mBq m $^{-3}$, $n = 4$: Yamada et al., 2006) and the Japan Sea (8 – 25 mBq m $^{-3}$: Kang et al., 1997; Hirose et al., 1999, 2002; Yamada and Zheng, 2008). The horizontal and vertical distribution patterns of both Pu activity and the isotopic ratio have all pointed towards the SCS receiving Pu from far field transport originated from the PPG via the NEC and Kuroshio Current. Moreover, the feeding to the SCS of Pu from PPG release has continuously existed and the PPG contribution to the SCS was estimated to be $41 \pm 17\%$. The Pu isotopic compositions in both surface water and deep water revealed faster scavenging of Pu sourced from the PPG and higher accumulation of Pu in the SCS compared to the Kuroshio. Furthermore, the Pu scavenging efficiencies in the SCS basin and the NSCS shelf were correspondingly estimated to be $\sim 11.6\%$ (9.1 – 13.6%) and $\sim 69.6\%$ (36.4 – 92.8%) through comparison of the $^{239} + ^{240}\text{Pu}$ inventories between water column and sediment core. It is important to note that these estimates have some uncertainty due to the limited field data. Finally, from the activity level and atom ratio

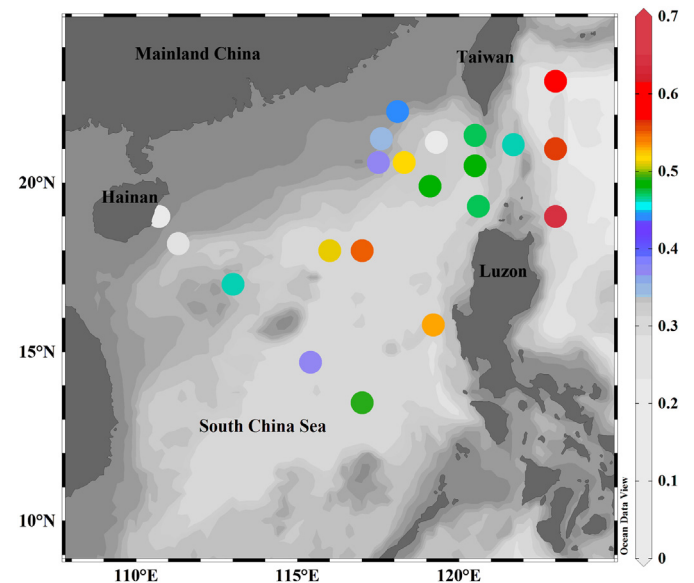


Fig. 7. Distribution of percentage contribution of Pu from the Pacific Proving Grounds in the South China Sea and across the Luzon Strait.

of Pu isotopes in the SCS, we have established a baseline for future environmental risk assessment related to increasing nuclear power plant operations in the region.

Notes

The authors declare no competing financial interest.

Author contributions

The manuscript was written through the contributions of all authors. All authors have given approval to the final version of the manuscript.

Acknowledgements

This work was supported by the National Basic Research Program of China (2009CB421200), the Major National Scientific Research Project (2015CB954000) and the Kakenhi Grant-in-Aid for Scientific Research on Innovative Areas (24110004). The authors express their gratitude to Dr. Xianghui Guo, Dr. Weidong Zhai and Dr. Jinwen Liu for providing assistance in sample collection, and to Fan Zhang for providing assistance in sample analysis. The authors are also grateful to Zhouling Zhang for providing TSM data sets, and the crew of *Dongfanghong II* for providing much help during the cruises. Professor John Hodgkiss is thanked for polishing the English. Three anonymous reviewers are thanked for their constructive comments and suggestions that have contributed to improve this paper.

References

- Adams, C.E., Farlow, N.H., Schell, W.R., 1960. The compositions, structures and origins of radioactive fallout particles. *Geochim. Cosmochim. Acta* 18, 42–56.
- Beasley, T.M., Kelley, J.M., Orlandini, K.A., Bond, L.A., Aarkrog, A., Trapeznikov, A.P., Pozolotina, V.N., 1998. Isotopic Pu, U and Np signatures in soils from Semipalatinsk-21, Kazakh Republic and the southern Urals, Russia. *J. Environ. Radioact.* 39, 215–230.
- Bowen, V.T., Noshkin, V.E., Livingston, H.D., Volchok, H.L., 1980. Fallout radionuclides in the Pacific Ocean: vertical and horizontal distribution, largely from GEOS-ES station. *Earth Planet. Sci. Lett.* 49, 411–434.
- Bu, W.T., Zheng, J., Guo, Q.J., Aono, T., Tagami, K., Uchida, S., Tazoe, H., Yamada, M., 2014a. Ultra-trace plutonium determination in small volume seawater by sector field inductively coupled plasma mass spectrometry with application to Fukushima seawater samples. *J. Chromatogr. A* 1337, 171–178.
- Bu, W.T., Zheng, J., Guo, Q.J., Aono, T., Tazoe, H., Tagami, K., 2014b. A method of measurement of ^{239}Pu , ^{240}Pu , ^{241}Pu in high U content marine sediments by sector field ICP-MS and its application to Fukushima sediment samples. *Environ. Sci. Technol.* 48, 534–541.
- Bu, W.T., Zheng, J., Guo, Q.J., Uchida, S., 2014c. Vertical distribution and migration of global fallout Pu in forest soils in southwestern China. *J. Environ. Radioact.* 136, 174–180.
- Buesseler, K.O., 1997. The isotopic signature of fallout plutonium in the North Pacific. *J. Environ. Radioact.* 36, 69–83.
- Buesseler, K.O., Dai, M.H., Aoyama, M., Benitez-Nelson, C., Charmasson, S., Hignley, K., Maderich, V., Masque, P., Morris, P.J., Oughton, D., Smith, J.N., 2017. Fukushima Daiichi-derived radionuclides in the ocean: transport, fate and impacts. *Annu. Rev. Mar. Sci.* 9, 173–203.
- Cai, P.H., Zhao, D.C., Wang, L., Huang, B.Q., Dai, M.H., 2015. Role of particle stock and phytoplankton community structure in regulating particulate organic carbon export in a large marginal sea. *J. Geophys. Res. Oceans* 120, 2063–2095.
- Centurioni, L.R., Niiler, P.P., Lee, D.K., 2004. Observations of inflow of Philippine Sea surface water into the South China Sea through the Luzon Strait. *J. Phys. Oceanogr.* 34, 113–121.
- Choppin, G.R., 2006. Actinide speciation in aquatic systems. *Mar. Chem.* 99, 83–92.
- Choppin, G.R., 2007. Actinide speciation in the environment. *J. Radioanal. Nucl. Chem.* 273, 695–703.
- Chou, W.C., Sheu, D.D.D., Chen, C.T.A., Wang, L.S., Tseng, C.M., 2005. Seasonal variability of carbon chemistry at the SEATS time-series site, Northern South China Sea between 2002 and 2003. *TAO* 16, 445–465.
- Dai, M.H., Buesseler, K.O., Pike, S.M., 2005. Plutonium in groundwater at the 100K-Area of the US DOE Hanford site. *J. Contam. Hydrol.* 76, 167–189.
- Dai, M.H., Cao, Z.M., Guo, X.H., Zhai, W.D., Liu, Z.Y., Yin, Z.Q., Xu, Y.P., Gan, J.P., Hu, J.Y., Du, C.J., 2013. Why are some marginal seas sources of atmospheric CO_2 ? *Geophys. Res. Lett.* 40:2154–2158. <http://dx.doi.org/10.1002/grl.50390>.
- Dai, M.H., Gan, J.P., Han, A., Kung, H.S., Yin, Z., 2014. Physical dynamics and biogeochemistry of the Pearl River plume. In: Bianchi, T., Allison, M., Cai, W.J. (Eds.), *Biogeochemical Dynamics at Major River-Coastal Interfaces: Linkages with Global Change*. Cambridge University Press, pp. 321–352.
- Dong, W., Zheng, J., Guo, Q.J., Yamada, M., Pan, S.M., 2010. Characterization of plutonium in deep-sea sediments of the Sulu and South China Sea. *J. Environ. Radioact.* 101, 622–629.
- Du, C.J., Liu, Z.Y., Dai, M.H., Kao, S.J., Cao, Z.M., Zhang, Y., Huang, T., Wang, L., Li, Y., 2013. Impact of the Kuroshio intrusion on the nutrient inventory in the upper northern South China Sea: insights from an isopycnal mixing model. *Biogeosciences* 10, 6419–6432.
- Falkowski, P.G., Biscaye, P.E., Sancetta, C., 1994. The lateral flux of biogenic particles from the eastern North American continental margin to the North Atlantic Ocean. *Deep-Sea Res.* II 41, 583–601.
- Godoy, M.L.D.P., Godoy, J.M., Roldao, L.A., Tauhata, L., 2009. Determination of total content and isotopic compositions of plutonium and uranium in environmental samples for safeguards purposes by ICP-MS. *J. Environ. Radioact.* 100, 613–625.
- Han, A.Q., Dai, M.H., Kao, S.J., Gan, J.P., Li, Q., Wang, L.F., Zhai, W.D., Wang, L., 2012. Nutrient dynamics and biological consumption in a large continental shelf system under the influence of both a river plume and coastal upwelling. *Limnol. Oceanogr.* 57, 486–502.
- Hirose, K., Amano, H., Baxter, M.S., Chaykovskaya, E., Chumichev, V.B., Hong, G.H., Isogai, K., Kim, C.K., Kim, S.H., Miyao, T., Morimoto, T., Nikitin, A., Oda, K., Pettersson, H.B.L., Povinec, P.P., Seto, Y., Tkalin, A., Togawa, O., Veletova, N.K., 1999. Anthropogenic radionuclides in seawater in the East Sea/Japan Sea: results of the first-stage Japanese-Korean-Russian expedition. *J. Environ. Radioact.* 43, 1–13.
- Hirose, K., Miyao, T., Aoyama, M., Igarashi, Y., 2002. Plutonium isotopes in the Sea of Japan. *J. Radioanal. Nucl. Chem.* 252, 293–299.
- Ito, T., Aramaki, T., Kitamura, T., Otsuka, S., Suzuki, T., Togawa, O., Kobayashi, T., Senju, T., Chaykovskaya, E.L., Karasev, E.V., Lishavskaya, T.S., Novichkov, V.P., Tkalin, A.V., Shcherbinin, A.F., Volkov, Y.N., 2003. Anthropogenic radionuclides in the Japan Sea: their distributions and transport processes. *J. Environ. Radioact.* 68, 249–267.
- Joseph, A.B., Gustafson, P.F., Russell, I.R., Schuert, E.A., Volchok, H.L., Tamplin, A., 1971. Sources of Radioactivity and Their Characteristics—Radioactivity in the Marine Environment. Washington, National Academy Sciences, pp. 6–41.
- Kang, D.J., Chung, C.S., Kim, S.H., Kim, K.R., Hong, G.H., 1997. Distribution of ^{137}Cs and $^{239,240}\text{Pu}$ in the surface waters of the East Sea (Sea of Japan). *Mar. Pollut. Bull.* 35, 305–312.
- Kao, S.J., Yang, J.Y.T., Liu, K.K., Dai, M.H., Chou, W.C., Lin, H.L., Ren, X.J., 2012. Isotope constraints on particulate nitrogen source and dynamics in the upper water column of the oligotrophic South China Sea. *Global Biogeochem. Cycles* 26, GB2033. <http://dx.doi.org/10.1029/2011GB004091>.
- Kelley, J.M., Bond, L.A., Beasley, T.M., 1999. Global distribution of Pu isotopes and ^{237}Np . *Sci. Total Environ.* 237–238, 483–500.
- Kershaw, P.J., Woodhead, D.S., Lovett, M.B., Leonard, K.S., 1995. Plutonium from European reprocessing operations—its behavior in the marine environment. *Appl. Radiat. Isot.* 46, 1121–1134.
- Kim, C.K., Kim, C.S., Chang, B.U., Choi, S.W., Chung, C.S., Hong, G.H., Hirose, K., Igarashi, Y., 2004. Plutonium isotopes in seas around the Korean Peninsula. *Sci. Total Environ.* 318, 197–209.
- Kinoshita, N., Sumi, T., Takimoto, K., Nagaoka, M., Yokoyama, A., Nakanishi, T., 2011. Anthropogenic Pu distribution in Tropical East Pacific. *Sci. Total Environ.* 409, 1889–1899.
- Krey, P.W., 1976. Remote Pu contamination and total inventories from Rocky Flats. *Health Phys.* 30, 209–214.
- Lee, S.H., Gastaud, J., Povinec, P.P., Hong, G.H., Kim, S.H., Chung, C.S., Lee, K.W., Pettersson, H.B.L., 2003. Distribution of plutonium and americium in the marginal seas of the northwest Pacific Ocean. *Deep-Sea Res.* II 50, 2727–2750.
- Lin, P.G., Hu, J.Y., Zheng, Q.A., Sun, Z.Y., Zhu, J., 2016. Observation of summertime upwelling off the eastern and northeastern coasts of Hainan Island, China. *Ocean Dyn.* 66, 387–399.
- Lindahl, P., Keith-Roach, M., Worsfold, P., Choi, M.S., Shin, H.S., Lee, S.H., 2010. Ultra-trace determination of plutonium in marine samples using multi-collector inductively coupled plasma mass spectrometry. *Anal. Chim. Acta* 671, 61–69.
- Lindahl, P., Worsfold, P., Keith-Roach, M., Andersen, M.B., Kershaw, P., Leonard, K., Choi, M.S., Boust, D., Lesueur, P., 2011. Temporal record of Pu isotopes in inter-tidal sediments from the northeastern Irish Sea. *Sci. Total Environ.* 409, 5020–5025.
- Liu, K.K., Chao, S.Y., Shaw, P.T., Gong, G.C., Chen, C.C., Tang, T.Y., 2002. Monsoon-forced chlorophyll distribution and primary production in the South China Sea: observations and a numerical study. *Deep-Sea Res.* I 49, 1387–1412.
- Liu, J.G., Clift, P.D., Yan, W., Chen, Z., Chen, H., Xiang, R., Wang, D.X., 2014. Modern transport and deposition of settling particles in the northern South China Sea: sediment trap evidence adjacent to Xisha Trough. *Deep-Sea Res.* I 93, 145–155.
- Liu, Z.F., Zhao, Y.L., Colin, C., Stattegger, K., Wiesner, M.G., Huh, C.A., Zhang, Y.P., Li, X.J., Sompongchaiyakul, P., You, C.F., Huang, C.Y., Liu, J.T., Siringan, F.P., Le, K.P., Sathiamurthy, E., Hantoro, W.S., Liu, J.G., Tuo, S.T., Zhao, S.H., Zhou, S.W., He, Z.D., Wang, Y.C., Bunsomboonsakul, S., Li, Y.L., 2016. Source-to-sink transport processes of fluvial sediments in the South China Sea. *Earth Sci. Rev.* 153, 238–273.
- McCubbin, D., Leonard, K.S., Greenwood, R.C., Taylor, B.R., 2004. Solid-solution partitioning of plutonium in surface waters at the Atomic Weapons Establishment Aldermaston (UK). *Sci. Total Environ.* 332, 203–216.
- Mocak, J., Bond, A.M., Mitchell, S., Scollary, G., 1997. A statistical overview of standard (IUPAC and ACS) and new procedures for determining the limits of detection and quantification: application to voltammetric and stripping techniques. *Pure Appl. Chem.* 69, 297–328.
- Muramatsu, Y., Hamilton, T., Uchida, S., Tagami, K., Yoshida, S., Robison, W., 2001. Measurement of $^{240}\text{Pu}/^{239}\text{Pu}$ isotopic ratios in the soil from the Marshall Islands using ICP-MS. *Sci. Total Environ.* 278, 151–159.
- Noshkin, V.E., Wong, K.M., Jokela, T.A., Brunk, J.L., Eagle, R.J., 1987. Plutonium and americium behavior in coral atoll environments. In: Conner, T.P., Burt, C.W., Duedall, I.A. (Eds.), *Ocean Processes in Marine Pollution*. Robert E. Krieger Publ. Co., Malabar, FL, pp. 159–174.

- Pham, M.K., Sanchez, J.A., Povinec, P.P., Andor, K., Arnold, D., Benmansour, M., Bikit, I., Carvalho, F.P., Dimitrova, K., Edrev, Z.H., Engeler, C., Fouche, F.J., Garcia-Orellana, J., Gasco, C., Gastaud, J., Gudelis, A., Hancock, G., Holm, E., Legarda, F., Ikaheimonen, T.K., Ilchmann, C., Jenkinson, A.V., Kanisch, G., Kis-Benedek, G., Kleinschmidt, R., Koukoulou, V., Kuhar, B., LaRosa, J., Lee, S.H., LePetit, G., Levy-Palomo, I., Liong-Wee-Kwong, L., Llauro, M., Maringer, F.J., Meyer, M., Michalik, B., Michel, H., Nies, H., Nour, S., Oh, J.S., Oregioni, B., Palomares, J., Pantelic, G., Pfitzner, J., Pilvio, R., Puskeiler, L., Satake, H., Schikowski, J., Vitorovic, G., Woodhead, D., Wyse, E., 2008. A new certified reference material for radionuclides in Irish Sea sediment (IAEA-385). *Appl. Radiat. Isot.* 66, 1711–1717.
- Pham, M.K., Betti, M., Povinec, P.P., Benmansour, M., Bungler, V., Drefvelin, J., Engeler, C., Flemal, J.M., Gasco, C., Guillevic, J., Gurriaran, R., Groening, M., Happel, J.D., Herrmann, J., Klemola, S., Kloster, M., Kanisch, G., Leonard, K., Long, S., Nielsen, S., Oh, J.S., Rieth, P.U., Ostergren, I., Pettersson, H., Pinhao, N., Pujol, L., Sato, K., Schikowski, J., Varga, Z., Varti, V.P., Zheng, J., 2011. A certified reference material for radionuclides in the water sample from Irish Sea (IAEA-443). *J. Radioanal. Nucl. Chem.* 288, 603–611.
- Pittauer, D., Tims, S.G., Froehlich, M.B., Fifield, L.K., Wallner, A., Mcneil, S.D., Fischer, H.W., 2017. Continuous transport of Pacific-derived anthropogenic radionuclides towards the Indian Ocean. *Sci. Rep.* 7:44679. <http://dx.doi.org/10.1038/srep44679>.
- Povinec, P.P., Pham, K.K., Sanchez-Cabeza, J.A., Barci-Funel, G., Bojanowski, R., Boshkova, T., Burnett, W.C., Carvalho, F., Chapeyron, B., Cunha, I.L., Dahlgaard, H., Galabov, N., Fifield, L.K., Gastaud, J., Geering, J.J., Gomez, I.F., Green, N., Hamilton, T., Ibanez, F.L., Ibn-Majah, M., Kanish, G., Kenna, T.C., Kloster, M., Korun, M., Liong-Wee-Kwong, L., La-Rosa, J.J., Lee, S.H., Levy-Palomo, I., Malatova, M., Maruo, Y., Mitchell, P., Murciano, I.V., Nelson, R., Nouredine, A., Oh, J.S., Oregioni, B., Le-Petit, G., Petterson, H.B.L., Reineking, A., Smedley, P.A., Suckow, A., Van-der-Struijs, T.D.B., Voors, P.I., Yoshimizu, K., Wyse, E., 2007. Reference material for radionuclides in sediment IAEA-384 (Fangataufa Lagoon sediment). *J. Radioanal. Nucl. Chem.* 273, 383–393.
- Qu, T.D., Giron, J.B., Whitehead, J.A., 2006. Deepwater overflow through Luzon Strait. *J. Geophys. Res.* 111, C01002. <http://dx.doi.org/10.1029/2005JC003139>.
- UNSCEAR, 2000. Report: Sources and effects of ionizing radiation. United Nations Scientific Committee on the Effects of Atomic Radiation Exposures to the Public From Man-made Sources of Radiation. United Nations, New York.
- Schroeder, A., Wiesner, M.G., Liu, Z.F., 2015. Fluxes of clay minerals in the South China Sea. *Earth Planet. Sci. Lett.* 430, 30–42.
- Shaw, P.T., 1991. The seasonal variation of the intrusion of the Philippine sea water into the South China Sea. *J. Geophys. Res.* 94, 18213–18226.
- Shaw, P.T., Chao, S.Y., 1994. Surface circulation in the South China Sea. *Deep-Sea Res.* 41, 1663–1683.
- Sholkovitz, E.R., 1983. The geochemistry of plutonium in fresh and marine water environments. *Earth Sci. Rev.* 19, 95–161.
- Tian, J.W., Yang, Q.X., Liang, X.F., Xie, L.L., Hu, D.X., Wang, F., Qu, T.D., 2006. Observation of Luzon strait transport. *Geophys. Res. Lett.* 33, L19607. <http://dx.doi.org/10.1029/2006GL026272>.
- Tsumune, D., Aoyama, M., Hirose, K., 2003. Numerical simulation of ^{137}Cs and $^{239,240}\text{Pu}$ concentrations by an ocean general circulation model. *J. Environ. Radioact.* 69, 61–84.
- Wang, G., Xie, S.P., Qu, T., Huang, R.X., 2011. Deep South China Sea circulation. *Geophys. Res. Lett.* 38, L05601. <http://dx.doi.org/10.1029/2010GL046626>.
- Wei, C.L., Lin, S.Y., Sheu, D.D.D., Chou, W.C., Yi, M.C., Santschi, P.H., Wen, L.S., 2011. Particle-reactive radionuclides (^{234}Th , ^{210}Pb , ^{210}Po) as tracers for the estimation of export production in the South China Sea. *Biogeosciences* 8, 3793–3808.
- Weimer, W.C., Langford, J.C., 1978. Iron-55 and stable iron in oceanic aerosols: forms and availability. *Atmos. Environ.* 12, 1201–1205.
- Wong, G.T.F., Chao, S.Y., Li, Y.H., Shiah, F.K., 2000. The Kuroshio edge exchange processes (KEEP) study— an introduction to hypotheses and highlights. *Cont. Shelf Res.* 20, 335–347.
- Wong, G.T.F., Chung, S.W., Shiah, F.K., Chen, C.C., Wen, L.S., Liu, K.K., 2002. Nitrate anomaly in the upper nutricline in the northern South China Sea—evidence for nitrogen fixation. *Geophys. Res. Lett.* 29:2097. <http://dx.doi.org/10.1029/2002GL015796>.
- Wu, F.C., Zheng, J., Liao, H.Q., Yamada, M., 2010. Vertical distribution of plutonium and ^{137}Cs in lacustrine sediments in northwestern China: quantifying sediment accumulation rates and source identifications. *Environ. Sci. Technol.* 44, 2911–2917.
- Wu, J.W., Zheng, J., Dai, M.H., Huh, C.A., Chen, W.F., Tagami, K., Uchida, S., 2014. Isotopic composition and distribution of plutonium in northern South China Sea sediments revealed continuous release and transport of Pu from the Marshall Islands. *Environ. Sci. Technol.* 48, 3136–3144.
- Wu, K., Dai, M.H., Chen, J.H., Meng, F.F., Li, X.L., Liu, Z.Y., Du, C.J., Gan, J.P., 2015. Dissolved organic carbon in the South China Sea and its exchange with the Western Pacific Ocean. *Deep-Sea Res.* 112, 41–51.
- Yamada, M., Zheng, J., 2008. Determination of $^{240}\text{Pu}/^{239}\text{Pu}$ atom ratio in coastal surface seawaters from the western North Pacific Ocean and Japan Sea. *Appl. Radiat. Isot.* 66, 103–107.
- Yamada, M., Zheng, J., 2010. Temporal variation of $^{240}\text{Pu}/^{239}\text{Pu}$ atom ratio and $^{239} + ^{240}\text{Pu}$ inventory in water column of the Japan Sea. *Sci. Total Environ.* 408, 5951–5957.
- Yamada, M., Zheng, J., 2011. Determination of $^{240}\text{Pu}/^{239}\text{Pu}$ atom ratio in seawaters from the East China Sea. *Radiat. Prot. Dosim.* 146, 311–313.
- Yamada, M., Zheng, J., 2012. ^{239}Pu and ^{240}Pu inventories and $^{240}\text{Pu}/^{239}\text{Pu}$ atom ratios in the equatorial Pacific Ocean water column. *Sci. Total Environ.* 430, 20–27.
- Yamada, M., Zheng, J., Wang, Z.L., 2006. ^{137}Cs , $^{239} + ^{240}\text{Pu}$ and $^{240}\text{Pu}/^{239}\text{Pu}$ atom ratios in the surface waters of the western North Pacific Ocean, eastern Indian Ocean and their adjacent seas. *Sci. Total Environ.* 366, 242–252.
- Yang, Q.X., Zhao, W., Liang, X.F., Tian, J.W., 2016. Three-dimensional distribution of turbulent mixing in the South China Sea. *J. Phys. Oceanogr.* 46, 769–788.
- Zeng, M., Liu, Y.X., Ouyang, S.J., Shi, H., Li, C.X., 2016. Nuclear energy in the post-Fukushima era: research on the developments of the Chinese and worldwide nuclear power industries. *Renew. Sust. Energ. Rev.* 58, 147–156.
- Zheng, J., Yamada, M., Wu, F.C., Liao, H.Q., 2009. Characterization of Pu concentration and its isotopic composition in soils of Gansu in the northwestern China. *J. Environ. Radioact.* 100, 71–75.
- Zheng, J., Tagami, K., Watanabe, Y., Uchida, S., Aono, T., Ishii, N., Yoshida, S., Kubota, Y., Fuma, S., Ihara, S., 2012. Isotopic evidence of plutonium release into the environment from the Fukushima DNPP accident. *Sci. Rep.* 2:304. <http://dx.doi.org/10.1038/srep00304>.
- Zhong, Y.S., Bracco, A., Tian, J.W., Dong, J.H., Zhao, W., Zhang, Z.W., 2017. Observed and simulated submesoscale vertical pump of an anticyclonic eddy in the South China Sea. *Sci. Rep.* 7:44011. <http://dx.doi.org/10.1038/srep44011>.